Available online at www.sciencedirect.com
SCIENCE DIRECT®
Physica A 338 (2004) 335–355
PHYSICA A
www.elsevier.com/locate/physa

Rhythm synchronization and chaotic modulation of coupled Van der Pol oscillators in a model for the heartbeat

Angela M. dos Santos*, Sergio R. Lopes, Ricardo L. Viana

Departamento de Física, Universidade Federal do Paraná, Curitiba, Paraná 81531-990, Brazil

Received 18 September 2003

Abstract

We investigate a phenomenological model for the heartbeat consisting of two coupled Van der Pol oscillators. The coupling between these nodes can be both unidirectional or bidirectional, and an external driving produced by a pacemaker is also included in this model. In order to warrant a robust operation, it is desirable that both units oscillate in a synchronized way, even though in the presence of external influences or parameter mismatches which are unavoidable in a physiological setting. We study the synchronization properties of such an association with respect to the nature and intensity of coupling. We analyze in particular the (generalized) synchronization of rhythms characterized by a chaotic modulation of the oscillator frequencies. We also investigate the shadowing breakdown of numerically generated chaotic trajectories of the coupled oscillator system via unstable dimension variability in its chaotic invariant set.

PACS: 47.52.+j; 05.45.jn; 05.45.Xt

Keywords: Synchronization; Van der Pol equation; Coupled oscillators

1. Introduction

The idea of treating the heart as a system of coupled nonlinear oscillators dates back from 1928, when Van der Pol and Van der Mark [1] simulated a heartbeat with three coupled electronic systems exhibiting relaxation oscillations. They were able to actually build such circuits, in which the "heartbeat" was represented by the flashing of a diode

* Corresponding author.
E-mail address: ansantos@fisica.ufpr.br (A.M. dos Santos).

0378-4371/$ - see front matter
doi:10.1016/j.physa.2004.02.058

vacuum tube, after the circuit component values were adjusted to give an oscillation period of 1 s. The time series of the voltage fluctuations was, in fact, reminiscent of an actual electrocardiogram (ECG). Accordingly, the Van der Pol equation, originally conceived to describe relaxation oscillators in electronic circuits, has been frequently used in theoretical models of the heart function [2,3].

The Van der Pol equation is a useful phenomenological model for the heartbeat, since it displays many of those features supposedly occurring in the biological setting, as complex periodicity, entrainment, and chaotic behavior [4]. The specific choice of the Van der Pol equation for this purpose is dictated by some criteria [2]: (i) the Van der Pol equation show parametric simplicity, in such a way that we can model the relationship between the period of oscillation and the parametric values in a simple way; (ii) each oscillator, when uncoupled from the others, must present (for some parameter values) a unique and stable limit cycle, continuously dependent on the system parameters; (iii) the amplitude of the oscillation must be largely independent of the oscillation rate, so as to simplify the coupling of the oscillators; and finally (iv) the oscillator must be able to have a response in frequencies with different values, when compared with its natural or free frequency.

As a phenomenological model of the heartbeat, the Van der Pol equations are justifiable on the basis of the similarity of the qualitative features of the heart dynamics for all individuals [5], such that a simple equation could in principle describe qualitatively the dynamical features of interest, such as mode-locking, bifurcations, and chaos for example. This approach has been used in a variety of models, including discrete-time mappings [6]. Although no direct biophysical relation is taken with the dynamical variables of the Van der Pol equation, as it occurs, for example, with the heart models of Beeler-Reuter [7] and Noble [8], we may relate the dynamical variable with the action potential in the heart cells.

The normal cardiac rhythm is generated by a specialized aggregate of cells in the right atrium called sino-atrial (SA) node, which is considered the normal pacemaker [9]. In addition, there is another pacemaker, the atrio-ventricular (AV) node. Katholi and co-workers [2] have pioneered the use of coupled Van der Pol equations for describing the interaction between the rhythms generated by the SA and AV nodes, considering a feedback loop for the coupling between the SA and AV nodes, and analyzing the periodic behavior of the system. Engelbrecht and Kongas [10] have used driven quasi-periodic asymmetric Van der Pol equations to investigate the more complex dynamical features that can appear in such models, but without a specific coupling.

The SA node generates impulses which spread through the atrial musculature, the AV node, and conducting tissues to the ventricles. Moreover, the excitation of the atria and ventricles occurs with a time lag in the millisecond range. Certain disorders, called AV blocks, are related to many kinds of variations in these time lags [5]. This asymmetry in the roles of the SA and AV nodes should be reflected on the strongly unidirectional character of the coupling between these oscillators. Hence, we will take, as a first approximation, a unidirectional coupling from the SA to the AV node; and as a more accurate model a bidirectional but asymmetric coupling.

Other dynamical feature of coupled oscillators with potential applications in the studies of the heartbeat is the synchronization of periodic and chaotic motion [11]. Within

a given node, for example, we expect that the specialized cells must act in some synchronized way, either periodic or chaotic, in order to generate a single and coherent pulse for the entire node [9]. But we can also investigate the synchronization between the nodes themselves, since there has been recognized that the generation of cardiac dysrhythmias are associated with a lack of synchronization between autonomous pacemakers [5]. Moreover, the rhythms generated by these pacemakers compete for the control of the heartbeat, and can result in some kinds of heart diseases [6].

This study can also include an external pacemaker coupled to the SA node. In terms of our coupled Van der Pol oscillator model, this effect can be emulated by a periodic driving term on the SA oscillator [12]. Controlling irregular and chaotic heartbeats is a key issue in cardiology, underlying the experimental and clinical use of artificial pacemakers. There are many strategies of control, based either in the use of external sources of periodic or quasi-periodic signals, as well as the use of small perturbations to stabilize periodic orbits embedded in the chaotic dynamics [13,14].

In this paper we investigate a coupled system of Van der Pol oscillators describing the interaction between the SA and AV nodes, with a forcing term which stands for an external pacemaker. We would like to emphasize that this is not intended to be a realistic model of the heartbeat, since it lacks a proper physiological background. In particular, the number of model parameters is not enough to allow for comparisons with realistic ECG data. The literature presents other modeling approaches [15–17] with such attributes. An important issue that can be raised when considering healthy heartbeat dynamics is the question of fractal and scaling properties of oscillators [18–20]. Finally, we mention the existence of stochastic approaches for modelling dynamical patterns in heartbeats [21,22].

The main question to be discussed in this paper is the dependence of the synchronization properties of the system with respect to the intensity and directionality of the coupling. We have found the occurrence of many kinds of synchronization [23]. Phase synchronization, however, was not observed in our system due to the large mismatch of normal modes of the oscillators [24].

On the other hand, the high dimensionality of the coupled oscillator system, combined with the observed existence of chaotic dynamics, raises the question of shadowability of numerical trajectories: are the computer-generated chaotic trajectories of our model closely followed, or shadowed, by "true" chaotic trajectories? The answer is affirmative, for arbitrarily long times, only for hyperbolic dynamical systems [25,26]. The coupled Van der Pol oscillator system fails to be hyperbolic, so that the shadowability of numerical trajectories cannot be assured a priori [27]. Moreover, there are parameter intervals for which the system presents a mathematical property called *unstable dimension variability* [28], which represents a severe mechanism of shadowing breaking of numerical trajectories [29]. We investigate in this paper the existence of parameter intervals where there is shadowing breakdown via unstable dimension variability by studying the behavior of the finite-time Lyapunov exponent closest to zero [30].

The rest of the paper is organized as follows: Section 2 introduces the theoretical model of coupled Van der Pol oscillators, as well as the basic concepts to be used in the discussion of synchronization. Section 3 considers the case of unforced

oscillators with unidirectional coupling. Section 4 analyzes the effect of a forcing term and bidirectional coupling. The behavior of the finite-time Lyapunov exponents, in order to investigate the shadowing breakdown of chaotic trajectories of the coupled oscillators, is treated in Section 5. The last section contains our conclusions.

2. Coupled Var der Pol oscillators and their synchronization

The oscillations of both the sino-atrial and atrio-ventricular nodes will be described by a set of two coupled Van der Pol equations, written in the general form of a pair of Liénard equations as

$$\dot{x_1} = x_2 \ , \tag{1}$$

$$\dot{x_2} = k(x_1 - w_1)(x_1 - w_2)x_2 - b_1 x_1 + a_1 \sin(f_1 t) + c_1(x_3 - x_1) \ , \tag{2}$$

$$\dot{x_3} = x_4 \ , \tag{3}$$

$$\dot{x_4} = k(x_3 - w_1)(x_3 - w_2)x_4 - b_2 x_3 + c_2(x_1 - x_3) \ , \tag{4}$$

where the pairs of variables (x_1, x_2) and (x_3, x_4) refer to the SA and AV nodes, respectively. The normal mode frequencies of the oscillators are denoted $b_1 > 0$ and $b_2 > 0$, and the non-linearity of the node dynamics is represented by a quadratic function, such that $w_1 < 0$ and $w_2 > 0$ [10]. The values $k = -1.45$, $w_1 = -0.2$, and $w_2 = 1.9$ will be used throughout this work.

The driving term, with amplitude $a_1 > 0$ and frequency $f_1 > 0$ may represent an externally fed pacemaker coupled to the SA node. Moreover, we have considered two "diffusive" coupling types: (a) $c_1 = 0$, $c_2 > 0$, representing an unidirectional coupling; and (b) $c_1 > 0$, $c_2 > 0$, with $c_1 \ll c_2$ for an asymmetric bidirectional coupling.

When unforced and uncoupled to the AV node ($c_1 = c_2 = a_1 = 0$), the SA node undergoes periodic regular oscillations, according to the usual mechanism of relaxation oscillators: the damping is counterbalanced by the "negative resistance" effect of the nonlinear term, and the result is a stable limit cycle in the phase plane (x_1, x_2) (see Fig. 1) [31]. The stability of these regular oscillations is necessary for the robustness of the heartbeat with respect to variations in external conditions.

The dynamics of a regular oscillation of the SA node does not depend so much of their amplitudes but rather on their phases, as has been stressed by the works of Glass and collaborators [5]. In the limit, a satisfactory model for some aspects of the heartbeat is simply a circle map $\theta \mapsto f(\theta)$ of $[0, 2\pi)$ into itself [6]. In the context of the present discussion, it is easy to associate a phase to the oscillations of both the SA and AV nodes, such that shown in Fig. 1. If the limit cycle encircles the origin of the phase plane (otherwise this can be done by a simple translation of axis), geometrical phases can be defined as

$$\theta_1(t) = \arctan\left(\frac{x_2(t)}{x_1(t)}\right) \ , \tag{5}$$

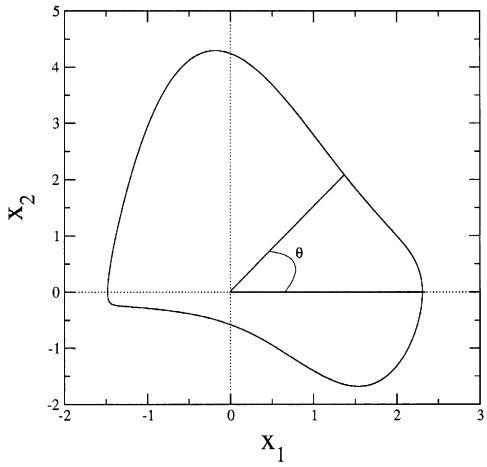

Fig. 1. Limit cycle in the (x_1, x_2) phase plane of the uncoupled and unforced SA node with $b_1 = 1.0$.

$$\theta_2(t) = \arctan\left(\frac{x_4(t)}{x_3(t)}\right) \tag{6}$$

for the SA and AV nodes, respectively. The advantage of this procedure is that, even though the oscillations themselves may be chaotic, if the respective attractor still encircles the origin, geometrical phases can still be defined. If this is not the case, however, there are other ways to define a phase for the oscillations, either regular or chaotic, using Poincaré sections or Hilbert transform (the latter form is particularly appropriate to experimental data) [24].

In general, the time evolution of the phases of both nodes is monotonically increasing, with an average time rate called its winding number:

$$\Omega_i = \langle \dot{\theta}_i(t) \rangle = \lim_{T\to\infty} \frac{1}{T} \int_0^T \theta_i(t)\, \mathrm{d}t \quad (i = 1, 2) \tag{7}$$

and which can be given the natural meaning of endogenous frequencies for the oscillations generated by each node, assuming that the limit cycle exists at all. This definition holds as long as we can define the phases as in (5) and (6), even when the amplitudes are varying in a chaotic fashion.

As discussed in the introduction, it may be desirable to have synchronization between the oscillations of the SA and AV nodes, but the question shifts to what kind of synchronization should we hope for, at a given value of the coupling strength. Complete synchronization (CS) of oscillators, characterized by $x_1(t) = x_3(t)$ and $x_2(t) = x_4(t)$, is unlikely to be observed in practice, due to the non-similarity of the coupled oscillators [23]. In coupled oscillators with a small mismatch of the normal modes, and a coupling not too strong, it is also possible to observe a weaker effect called *lag synchronization* (LS), defined as the approximate equality (i.e., up to a small tolerance) of the state variables, but with a given time lag τ [32]:

$$x_1(t) \approx x_3(t - \tau), \quad x_2(t) \approx x_4(t - \tau)\,. \tag{8}$$

On the other hand, if the normal modes of the coupled Van der Pol oscillators are widely different, as in the case we are currently investigating, there is no longer LS, since the oscillator amplitudes are rather different. However, as we will see later on in this paper, the amplitudes can be delayed from each other from a constant time lag. This kind of behavior can be referred to as *rhythm synchronization* (RS).

A weaker form of synchrony between identical oscillators is *phase synchronization* (PS), for which the coupled system can undergo oscillations of widely different magnitudes, even chaotic ones, but with equal phases, $\theta_1(t) = \theta_2(t)$ [24,33]. For nearly identical systems, i.e., when they present a small parameter mismatch, this can be true up to a possibly small constant: $\theta_1(t) \approx \theta_2(t)$. Two systems exhibiting PS may not present CS, but the reverse is always true. It may also happen that, even when the phases themselves are not equal, their time rates are, which characterizes *frequency synchronization* (FS) $\Omega_1 \approx \Omega_2$ [34]. If the oscillator amplitudes are behaving periodically instead of chaotically, PS is nothing but mode-locking, or a commensurability between frequencies $m\Omega_1 - n\Omega_2 = 0$, where m and n are positive integers, which have been related to the Wenckebach periodicity observed in ECG recordings [3]. We also mention the possibility of *generalized synchronization* (GS), characterized by the existence of a functional relationship between the amplitudes of the two coupled oscillators, $x_2 = \mathscr{F}(x_1)$, and that may occur even for non-identical systems [35].

If the coupled systems were identical, a synchronization manifold $\mathscr{S}$ would be defined through the conditions $x_1 = x_3$ and $x_2 = x_4$. The CS state exists when $\mathscr{S}$ is asymptotically stable for all possible trajectories $\mathbf{s}(t) = (x_1(t), x_2(t))$ of the driving oscillator, either periodic or chaotic, against small displacements of the synchronized trajectories with respect to directions transversal to $\mathscr{S}$. The *conditional Lyapunov exponents* are the Lyapunov exponents of the response oscillator, $(x_3(t), x_4(t))$, under the explicit constraint that the exponents must be computed for points on the trajectory $\mathbf{s}(t)$ [23]. There are as many conditional exponents as the directions transversal to $\mathscr{S}$, but it suffices to compute the maximal conditional exponent λ_{cond}. The negativity of all conditional exponents is a necessary condition for the CS defined in $\mathscr{S}$ to be stable [23].

The autonomous four-dimensional vector field represented by the coupled Van der Pol equations (1)–(4), with a_1=0, has four Lyapunov exponents $\lambda_1 \equiv \lambda_{\max} > \lambda_2 > \lambda_3 > \lambda_4$. Chaotic and hyper-chaotic states are those for which $\lambda_1 > 0$ and $\lambda_1 > \lambda_2 > 0$, respectively. For uncoupled oscillators, and even for weakly coupled oscillators with phase coherent chaotic oscillators, there are two zero Lyapunov exponents linked to the individual phase evolutions. The onset of PS, or the vanishing of the phase difference $\theta_1 - \theta_2$ between them, is thus achieved when one of the two zero Lyapunov exponents undergoes a transition to negative values [23]. The second Lyapunov exponent, which vanishes for the uncoupled case, also becomes negative for stronger coupling, and the non-identical oscillators get correlated, yielding a nearly CS state.

3. Driven oscillators with unidirectional coupling

Let us first consider the simplest case, consisting of an autonomous SA node driving the oscillations of a AV node, without affecting back the SA node, in the typical

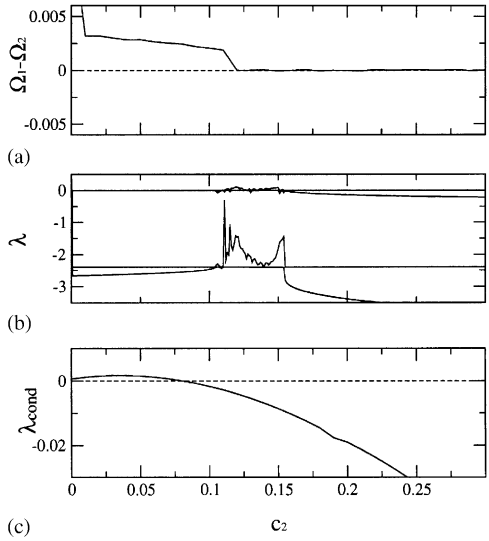

Fig. 2. (a) Frequency difference of two coupled Van der Pol oscillators as a function of the coupling strength c_2; (b) Lyapunov exponents; (c) Conditional Lyapunov exponent. The other parameter values are $b_1 = 1.0$, $b_2 = 0.666$.

form of a driver–response system ($a_1 = c_1 = 0$). The variable parameter will be taken as c_2, the strength of the unidirectional coupling, all the remaining parameters being held constant. We investigate in this section what is the effect of the coupling on the dynamics of the AV node.

Fig. 2(a) shows the variation of the frequency difference $\Omega_1 - \Omega_2$ with the coupling strength. As a general trend, as the latter increases the frequency difference decreases and, for $c_2 > c_2^* \approx 0.12$, this difference practically vanishes and the oscillators exhibit FS. In order to check whether or not the amplitudes are behaving chaotically, we also depicted in Fig. 2(b) the corresponding Lyapunov spectrum; and, to understand the various transitions to synchronized behavior, we plot in Fig. 2(c), the maximal conditional exponent λ_{cond}. The Lyapunov spectrum indicates that, within the interval $0.11 \lesssim c_2 \lesssim 0.15$ the dynamics is weakly chaotic. Hence, for $c_2 > 0.15$, FS is basically a manifestation of mode-locking, specially for strong coupling, but there are subintervals of non-zero measure for which FS occurs even with chaotic amplitudes.

Since the oscillators representing the SA and AV nodes are non-identical, some caution is needed when applying concepts originally derived for identical coupled systems. For example, as we mentioned at the end of Section 2, the negativity of the conditional exponent is a necessary, but not sufficient condition for CS. In fact, Fig. 3(a) shows a x_1–x_3 projection of the phase space of the coupled system for $c_2 = 0.12$, where $\lambda_{\max} > 0$ [cf. Fig. 2(b)], but $\lambda_{cond} < 0$ [cf. Fig. 2(c)] and, in spite of this, there is no CS state. The explanation lies in the fact that, since the coupled systems are not identical, there is no synchronization manifold, but $\lambda_{cond} < 0$ characterizes the global stability of the

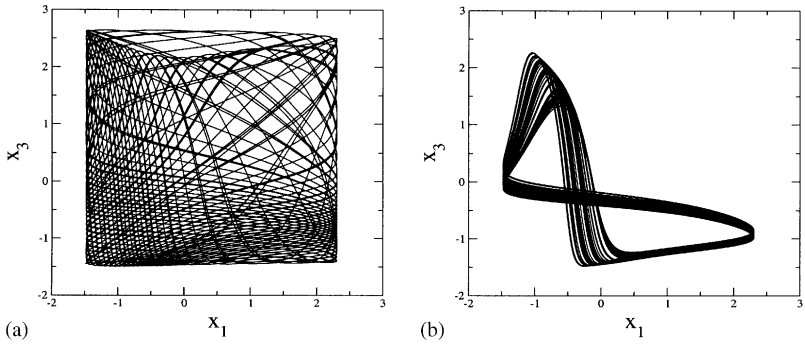

Fig. 3. Projection of the phase space for (a) $c_2 = 0.12$; (b) $c_2 = 0.15$.

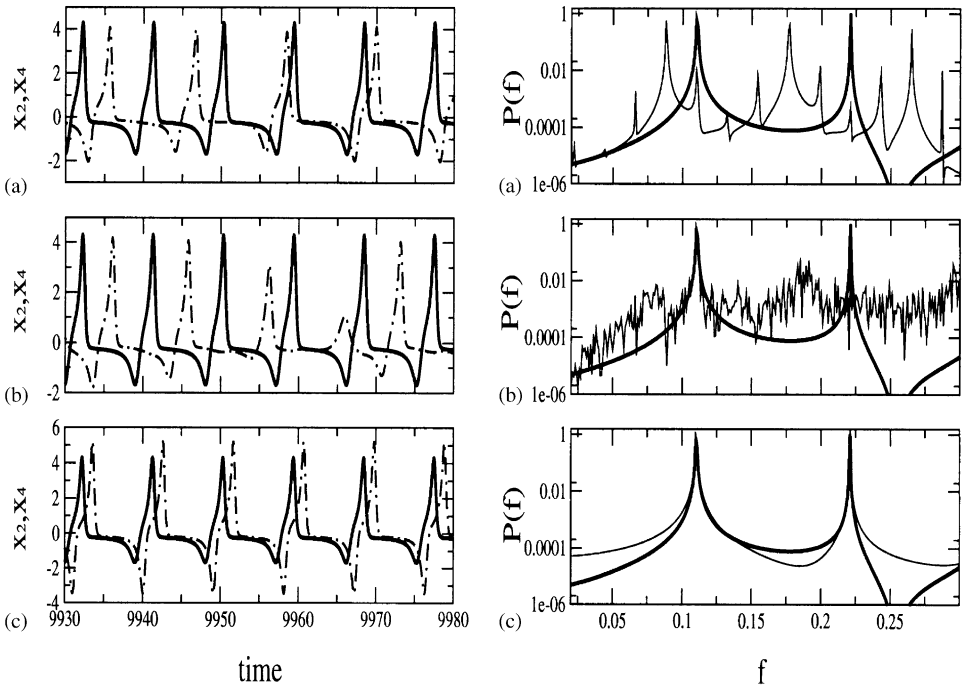

Fig. 4. Left: Time series of x_2 (full lines) and x_4 (dashed lines) for $c_2 =$ (a) 0.05; (b) 0.12; and (c) 0.48. Right: power spectral density corresponding to the time series of x_2 (bold curve) and x_4 (light curve).

attractor. For higher coupling, however, the coherence between oscillator amplitudes is improved, and a GS state is developed [Fig. 3(b)].

Fig. 4 shows time series for the oscillator time rates x_2 and x_4 and the corresponding power spectra. Weak coupling [Fig. 4(a), for $c_2 = 0.05$] does not lead to synchronization,

as expected from our previous analysis, the successive peaks occurring at varying intervals and with unequal amplitudes. For c_2 at the threshold of FS, [Fig. 4(b), for $c_2 = 0.12$] when one of the Lyapunov exponents indicates chaos, we see that, whereas the amplitudes of the driver oscillator (the SA node) are fixed, the amplitudes of the slave oscillator (the AV node) have irregularly fluctuating values. A feature present in Fig. 4(b) is the *chaotic modulation* of the oscillator frequencies.

Chaotic modulation is characterized by a periodic driver behavior, combined with a chaotic dynamics of the response oscillator, such that the latter has a broadband power spectrum, but with frequency peaks which coincide with those of the periodic driver oscillator. Once the intervals between the amplitude peaks of both oscillators are nearly constant with time, chaotic modulation is also implying rhythm synchronization (RS). A situation where the coupling is stronger [Fig. 4(c), for $c_2 = 0.48$] exhibits a *generalized lag synchronized* (GLS) state, since there is a nearly constant time interval between peaks (the time lag) [23]. This is not a pure LS case, though, for the oscillator amplitudes are significantly different. The frequencies themselves, on the other hand, practically coincide in the power spectrum. Since the motion is strictly periodic in this case, one could classify this behavior as a *lagged mode-locking*. Since we relate generalized synchronization to a functional relationship between the signals, in Fig. 5 we show the phase-space projections x_2–x_4 corresponding to the three cases shown in Fig. 4. Observe that such a relationship is clearly shown in Fig. 5(c).

The presence of LS can be numerically diagnosed by computing the similarity function, which is the time averaged difference between the variables of each oscillator (subtracted from their mean values), and taken with a time shift τ [32]

$$S_{ij}^2(\tau) = \frac{\langle [\tilde{x}_2(t+\tau) - \tilde{x}_4(t)]^2 \rangle}{[\langle \tilde{x}_2^2(t) \rangle \langle \tilde{x}_4^2(t) \rangle]^{1/2}}\,, \tag{9}$$

where $\tilde{x}_i = x_i - \langle x_i \rangle, i = 2, 4, \langle \cdots \rangle$ being the mean value over a sufficiently large time interval [32]. For completely non-synchronized and independent time series, we have that $S(\tau) \sim 1$ for all time lags. On the other hand, let us denote τ_0 the time delay for which this similarity function has a minimum value S_0. If we have a LS state, the similarity function must decrease to zero (its minimum value) for $\tau_0 = 0$, whereas a generalized LS implies the existence of a minimum S_0, but this time for a *non-zero* lag τ_0.

Fig. 6 shows the dependence of the similarity function on the time shift for the same cases depicted in Fig. 4. A non-synchronized state (curve 1, for $c_2 = 0.05$) shows a nearly constant value of the similarity function ($S \approx 1.4$) for a wide range of lags. This can be understood by observing that, if x_2 and x_4 are mutually independent variables, their difference is of the same order as the variables themselves. The same happens to a state for which RS state occurs (curve 2, for $c_2 = 0.14$). On the other hand, the similarity function for $c_2 = 0.48$ (curve 3) presents a minimum $S_0 \approx 0.35$ at a time lag $\tau_0 \approx 1.3 \neq 0$, indicating a case of GLS.

As a general rule, for identical systems (where the frequencies are perfectly matched) and with a unidirectional coupling, the sequence of synchronization types, in decreasing order of coupling, is: CS $\rightarrow$ LS $\rightarrow$ GS $\rightarrow$ PS $\rightarrow$ non-synchronized behavior [23]. If there is a small non-zero frequency mismatch, the sequence changes to: CS $\rightarrow$ PS $\rightarrow$

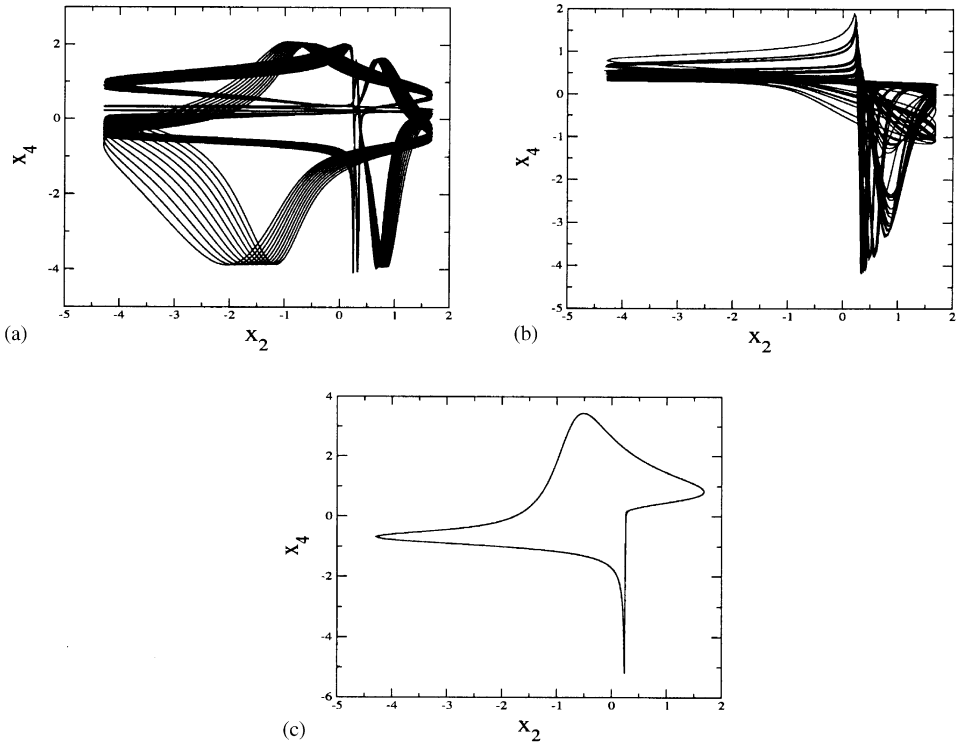

Fig. 5. Projection of the phase space for $c_2=$ (a) 0.05; (b) 0.12; and (c) 0.48.

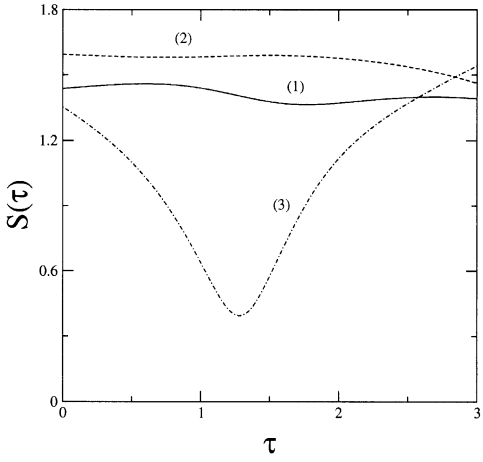

Fig. 6. Similarity function for varying time lag for $c_2 = 0.05$ (1); 0.12 (2); and 0.48 (3).

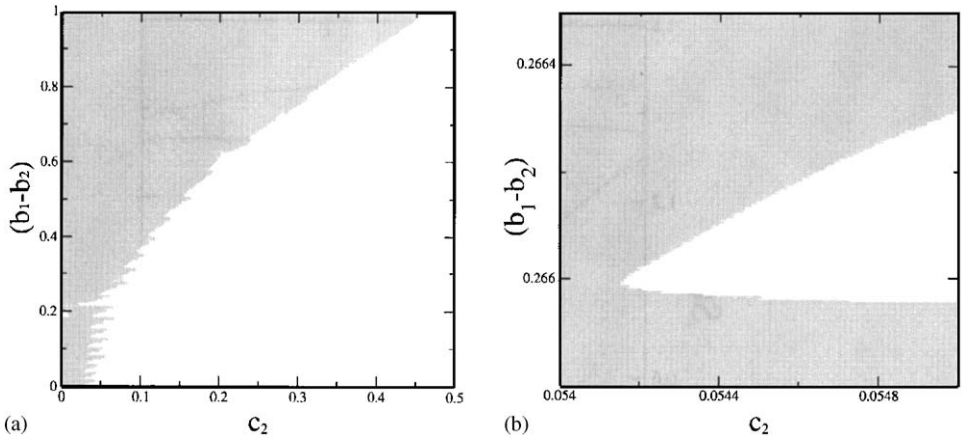

Fig. 7. (a) Synchronization regions in the parameter plane of normal mode frequency mismatch versus coupling strength. White (gray) regions represent parameter values for which the conditional exponent λ_{cond} is negative (positive), (b) Magnification of the tip of one Arnold' tongue.

RS $\rightarrow$ GLS $\rightarrow$ non-synchronized behavior. On the other hand, if the frequencies are very different from each other, as in the problem we are investigating here, we have: CS $\rightarrow$ RS directly, without a PS stage, and it has been conjectured that it would end up with a GLS state [36].

We can follow how these transitions occur, as some other oscillator parameter varies, such as the difference b_1-b_2 between normal mode frequencies of both oscillators. In Fig. 7(a) white pixels represent parameter values for which $\lambda_{cond} < 0$, i.e., these parameter values lead to GS states; whereas gray pixels stand for positive conditional exponents and, consequently, to non-synchronized states. The boundary between GS and non-synchronized regions is a wiggled line which, in finer scales, resembles a set of Arnold tongues for a single, periodically forced oscillator, where the frequency is b_1-b_2 and the nonlinearity strength is proportional to the coupling c_2. A magnification of the tip of one of those tongues is shown in Fig. 7(b).

4. Forced oscillators and bidirectional coupling

In this section, we investigate some effects of adding an external periodic driving in the oscillator describing the SA node, which can represent the effect of a pacemaker which imparts a sinusoidal signal to the oscillator regardless of its phase. An actual pacemaker would take into account the inter-beat intervals in order to trigger a signal which can anticipate the heartbeat whenever necessary [37]. In terms of our coupled system of Van der Pol oscillators, the addition of an external driving may be regarded as a third oscillator, which is the ultimate driver, the SA and AV nodes being just the corresponding responses to this invariably periodic driving. This approach has been used to describe synchronization between a chaotic oscillator with a periodic driving [24].

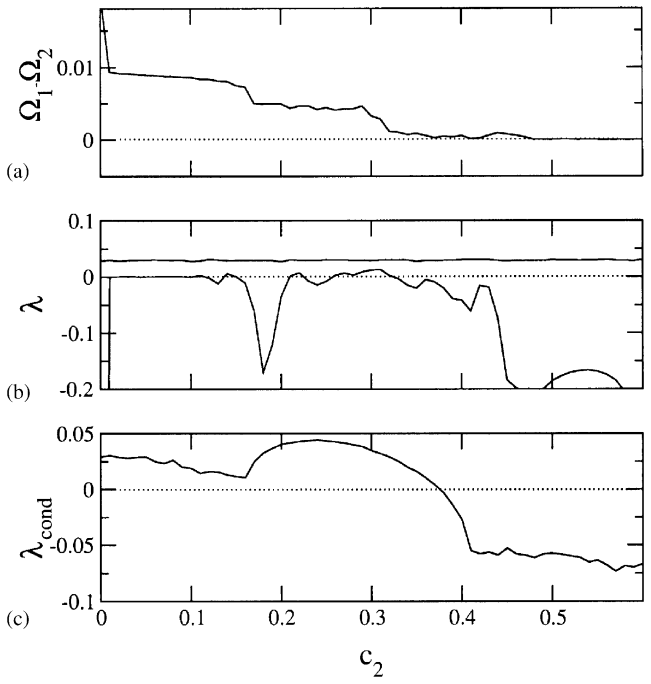

Fig. 8. (a) Frequency difference of two coupled Van der Pol oscillators with external forcing as a function of the coupling strength c_2; (b) Lyapunov exponents; (c) Conditional Lyapunov exponent. The other parameter values are $a_1 = 0.95$, $b_1 = 1.0$, $b_2 = 0.666$.

Fig. 8 shows an example of driving with amplitude $a_1 = 0.95$ and frequency $f_1 = 1.0$. Many aspects of the unforced cases are still seen here, as the decrease of the frequency difference with the coupling strength. The transition to FS occurs at $c_2 = 0.4$ [Fig. 8(a)], which is much greater than the corresponding threshold for the unforced case, namely, 0.12, due to the driving frequency being considerably greater than the normal mode frequencies. Hence, the coupling should be more intense to make the response oscillators to synchronize with the driving oscillator. In other words, the coupled system increases its frequency mismatch in the bidirectional case.

The presence of chaotic behavior for a wide range of coupling strengths can be ascribed to the driving effect (in fact, for some values of c_2 it exhibits even hyper-chaos) [Fig. 8(b)]. The vanishing of the conditional exponent, indicating the onset of a chaotic GLS state, occurs at $c_2 \approx 0.38$ [Fig. 8(c)]. This anomalous behavior of the conditional Lyapunov exponent λ_{cond} is due to the presence of hyper-chaos. The transition from non-synchronized to synchronized states in the forced case is more complex though, as revealed by Fig. 9, which plots the regions for which λ_{cond} is positive or negative in the parameter plane (coupling strength versus normal mode frequency mismatch). The boundary of the synchronized region is not as sharp as in Fig. 7 and, since the area

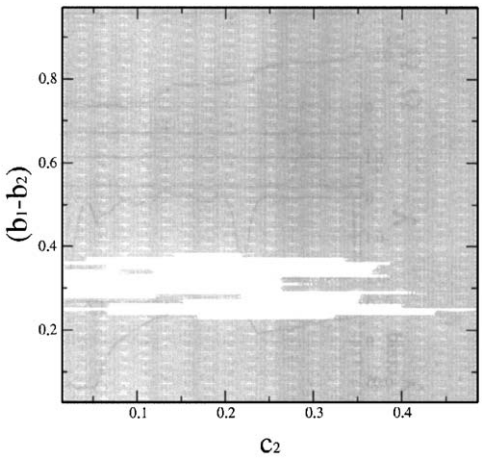

Fig. 9. Synchronization regions in the parameter plane of normal mode frequency mismatch versus coupling strength. White (gray) regions represent parameter values for which the conditional exponent λ_{cond} is negative (positive).

of the synchronized (white) region is comparatively small, synchronization of forced oscillators becomes less likely to occur.

The presence of multiple Arnold tongues can be inferred from Figs. 10(a) to (d), where we plot the frequency ratio Ω_2/Ω_1 as a function of the coupling strength, for different normal mode frequencies. We see that, for small coupling, there are plateaus of constant ratios, which are a characteristic feature of mode-locked regions represented by Arnold tongues in the parameter plane. The full lines in Fig. 10 are exponential fittings representing an overall tendency of the frequency ratio to approach unity, with increasing coupling strength. Hence, for strong coupling (large c_2), the response oscillator tends to adapt itself to the driving frequency, as it would be expected on general grounds.

Let us now consider a bidirectional coupling ($c_1 \neq 0$). As long as the second coupling strength c_1 is kept at a small value (which is justifiable on the basis of the strongly asymmetric coupling between the SA and AV nodes), we have the gross features of the unidirectional case preserved, with some quantitative changes. For example, Fig. 11 depicts bifurcation diagrams for the maximum values of the x_4 variable as a function of the first coupling strength c_2, for different values of the second coupling strength c_1. For vanishing of c_1 [Fig. 11(a)] the coupling is unidirectional, and the dynamical behavior is rich, presenting periodic and chaotic orbits, as well as bifurcations and crisis. As c_1 becomes different from zero [Fig. 11(b)] and increases [Fig. 11(c)], the parameter intervals for which there is chaos are reduced, the dynamics becoming more regular. We remark that, in the limit case where $c_1 = c_2$ (which is not of interest in terms of the heartbeat model here considered), the coupling becomes diffusive, and many results exist about CS states [38].

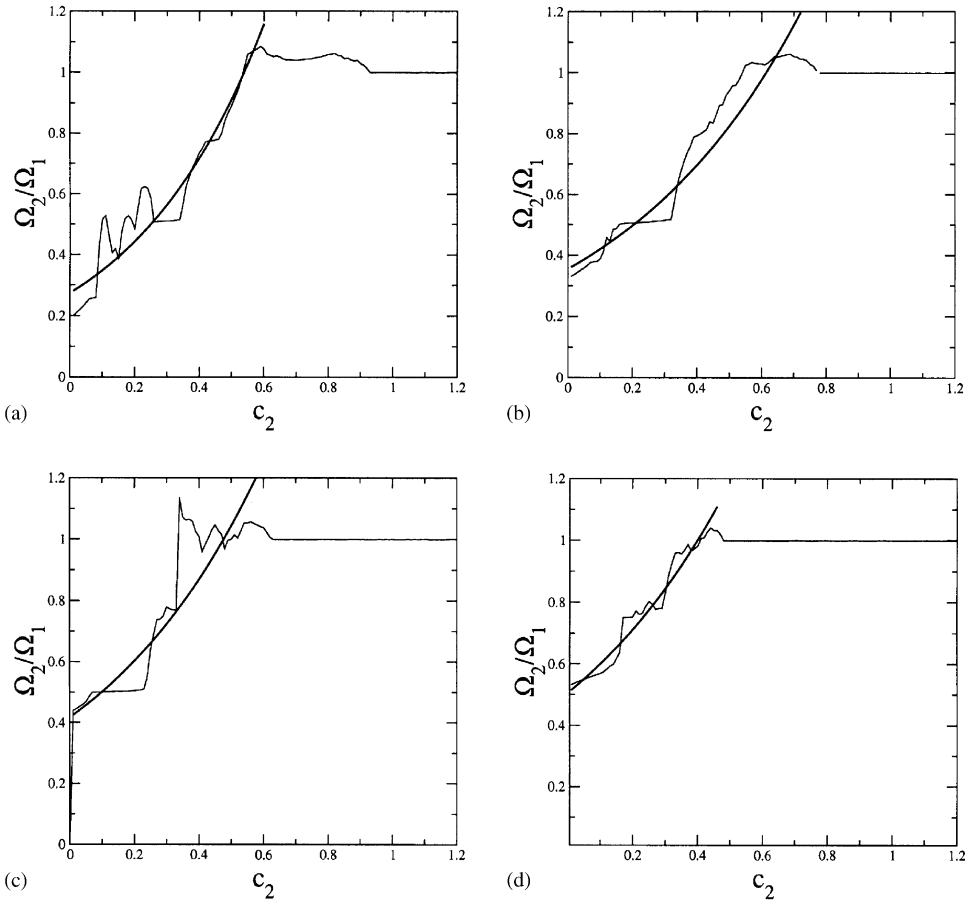

Fig. 10. Frequency ratios for the forced case as a function of the normal mode frequency, for $b_2 =$ (a) 0.166; (b) 0.33; (c) 0.5; and (d) 0.66

5. Finite-time Lyapunov exponents

Analyzing the diagram of Fig. 8(b) in the region $0.20 \lesssim c_2 \lesssim 0.35$, we see that the second Lyapunov exponent (λ_2) oscillates around zero, and this is related to a highly unstable region for the system dynamics. In fact, we can assign to this region a strongly non-hyperbolic behavior characterized by the existence of unstable periodic orbits, embedded in the chaotic attractor in the phase space, with a different number of unstable directions. This phenomenon has been called *unstable dimension variability* (UDV), and has profound consequences on the nature of the computer-generated chaotic trajectories of the system [28,30].

Computer-generated orbits are unavoidably subjected to very small one-step errors due to the use of finite-precision arithmetics, for example, or the use of a discretization

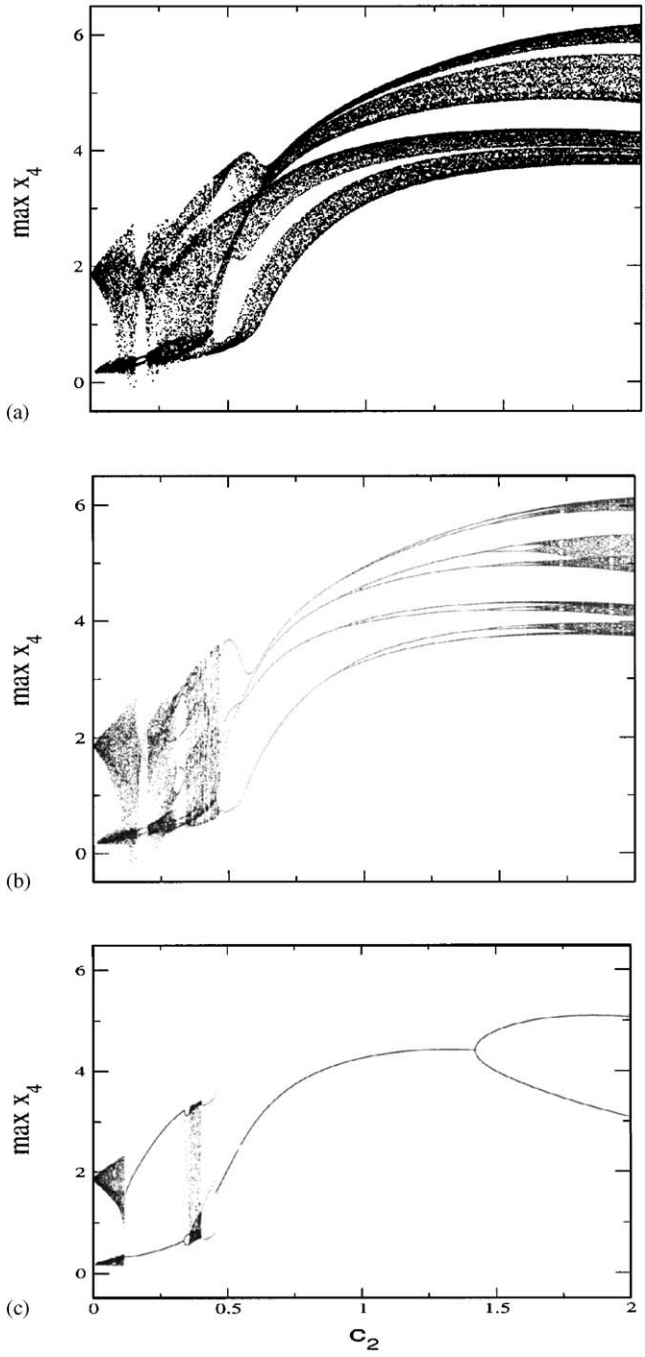

Fig. 11. Bifurcation diagrams for the maximum values of the variable x_4 as a function of the coupling strength c_2 for $c_1 =$ (a) 0.0; (b) 0.1; and (c) 0.5.

procedure by some numerical algorithm. Due to the intrinsic dynamical instability of chaotic orbits, we expect that these one-step errors cause an exponential divergence of the trajectories we produce, also called *pseudo-trajectories*. Hyperbolic chaotic systems have the important mathematical property that pseudo-trajectories are always followed closely, or *shadowed*, by true (i.e., noiseless) trajectories, such that, even though the trajectory we get is not that originally we sought for, it is arbitrarily close to a true trajectory which comes from another initial condition [25,26]. From the statistical point of view, it makes a little difference if we are using a pseudo or a true chaotic trajectory, what would gives us confidence on numerical computations of Lyapunov exponents, dimensions, entropies, etc.

This shadowability property holds, but for a finite time span only, for non-hyperbolic dynamical systems presenting homoclinic tangencies between stable and unstable manifolds [39]. If the non-hyperbolicity comes from UDV, however, it turns out that chaotic pseudo-trajectories are shadowed by true trajectories for extremely small time intervals. When the shadowability time is too small in comparison with the length of the phase-space trajectories we generate using computers, we cannot assure the validity of these trajectories, when taken isolately [40].

In the chaotic invariant set (e.g, a chaotic attractor) of a dynamical system exhibiting UDV there are unstable orbits with a different number of unstable eigen-directions. Hence, a typical chaotic orbit will experience in average expansions or contractions along some specified direction. This can be quantified by using finite-time Lyapunov exponents, which are computed in the usual way, but with a usually small time span [41]. A numerical fingerprint of UDV is the fluctuating behavior around zero of the finite-time exponent closest to zero [30].

The time-n Lyapunov exponents of flow (1)–(4) will be denoted $\lambda_k(\mathbf{x}_0, n)$, with $k = 1, 2, 3, 4$. The infinite time-limit of them reduces to the usual Lyapunov exponents $\lambda_k = \lim_{n\to\infty} \lambda_k(\mathbf{x}_0, n)$. Although the time-$n$ exponent $\lambda_k(\mathbf{x}_0, n)$ generally takes on a different value, depending on the value of $\mathbf{x}_0$ we choose, the infinite time limit takes on the same value for almost all $\mathbf{x}_0$ with respect to the natural ergodic measure of the invariant set [43]. In the coupled Van der Pol equation system we are considering in this work, the time-n exponent closest to zero is $\lambda_2(n)$. If the chaotic attractor displays UDV, it turns out that $\lambda_2(n)$ will erratically fluctuate about zero, what suggests the use of a probability density $P(\lambda_2(\mathbf{x}_0; n), n)$ for them, so that $P(\lambda_2(n), n)\mathrm{d}\lambda_2$ is the probability that this time-n exponent takes on a value between λ_2 and $\lambda_2 + \mathrm{d}\lambda_2$ for a given time span n [42]. The initial conditions $\mathbf{x}_0$ are randomly chosen according to the Lebesgue measure of the chaotic attractor.

From this probability distribution we can obtain moments of functions of the time-n exponent, as averages

$$\langle F(\lambda_2(\mathbf{x}_0, n))\rangle = \frac{\int_{-\infty}^{+\infty} F(\lambda_2(\mathbf{x}_0, n))P(\lambda_2(\mathbf{x}_0, n), n)\,\mathrm{d}\lambda_2}{\int_{-\infty}^{+\infty} P(\lambda_2(\mathbf{x}_0, n), n)\,\mathrm{d}\lambda_2}\,. \tag{10}$$

We can obtain a numerical approximation for this probability distribution by considering a large number of trajectories of length n, say $n = 50$, from initial conditions randomly chosen in the chaotic attractor. In Fig. 12 we show some distributions of time-50 exponents, obtained for different values of the bifurcation parameter c_2, which

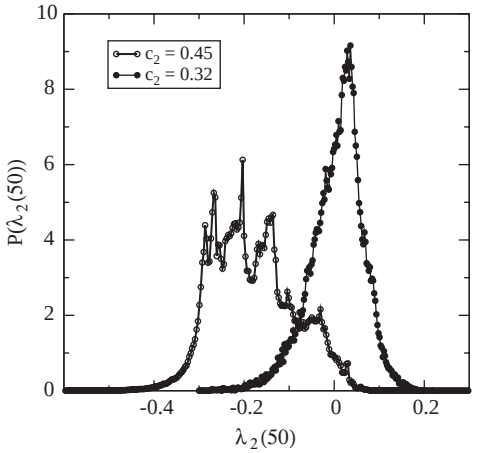

Fig. 12. Probability distribution for the time-50 exponent λ_2 and different values of the coupling strength c_2.

is the coupling constant. As c_2 decreases in the neighborhood of $c_2 = \tilde{c}_2 \approx 0.32$, the distribution as a whole drift toward positive values of $\lambda_2(50)$.

The chaotic attractor exhibits UDV in the neighborhood of this value, since there are contributions from $\lambda_2(50)$ with both positive and negative signs, indicating that there are pieces of chaotic trajectories which are attracted and repelled, in average, from the chaotic attractor. Hence, trajectories lying in the chaotic attractor are not shadowable for an appreciable time. These shadowability problems may not, however, spoil statistical quantities drawn from such chaotic trajectories, like averages and fluctuations. It has been proved for some dynamical systems of physical interest that, while single chaotic trajectories may present shadowability problems due to UDV, we can still obtain statistically relevant results using bunches of trajectories. This applies, for example, to calculations of entropies and dimensions [40].

It is useful to compute the relative number of positive finite-time Lyapunov exponents

$$\phi(n) = \frac{\int_0^{+\infty} P(\lambda_2(\mathbf{x}_0, n), n)\, \mathrm{d}\lambda_2}{\int_{-\infty}^{+\infty} P(\lambda_2(\mathbf{x}_0, n), n)\, \mathrm{d}\lambda_2} \tag{11}$$

depicted in Fig. 13 for the time-50 exponents considered in Fig. 12. The onset of UDV can be assigned to the point where this positive fraction begins to increase from zero [43,44]. In other words, UDV sets in when the distributions of $\lambda_2(50)$ start to develop a positive or negative tail, depending on what direction we take for varying the coupling strength. For example, Fig. 12 shows that, for $c_2 \gtrsim \tilde{c}_2$, the distribution $P(\lambda_2(50))$ have practically no positive values. Accordingly, Fig. 13 indicates that the fraction of positive values is nearly zero, and it suddenly goes to a value close to unity in a very steep ramp as c_2 crosses $\tilde{c}_2$, the latter value indicating a positive fraction of $\phi(50) = \frac{1}{2}$. For $c_2 \lesssim \tilde{c}_2$ the distribution has practically only positive values, having thus a tiny negative tail.

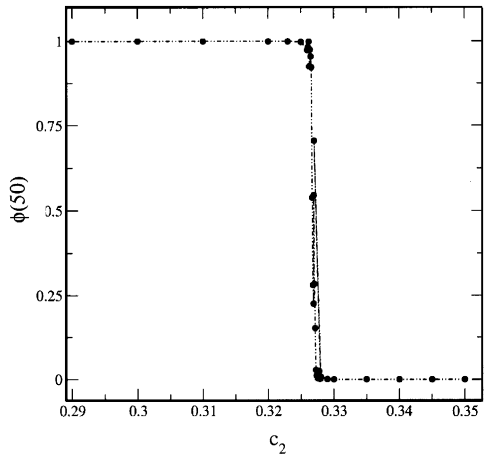

Fig. 13. Fraction of positive time-n Lyapunov exponent λ_2 in the vicinity of $\tilde{c}_2$.

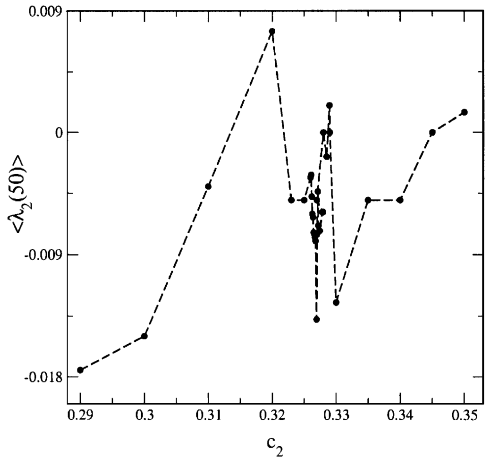

Fig. 14. Average time-50 Lyapunov exponent λ_2 as a function of the coupling strength c_2.

Another way to regard this transition is to compute the average value of $\lambda_2(50)$. Fig. 14 shows the evolution of the average value of the time-n exponents, $m = \langle \lambda_2(n) \rangle$, which is plotted versus the bifurcation parameter c_2. The critical point $\tilde{c}_2$, where the shadowing breakdown via UDV is most intense, can also be viewed as the value for which m crosses zero from above or below. However, we can also observe that there are other parameter intervals for which the average exponent crosses zero (at least three of them can be spotted in Fig. 14). Hence, the distribution of time-n exponents drifts in a complicated way as c_2 is swept through the range indicated by Fig. 14.

Finally, we would like to point out that the average shadowing time, i.e., the mean time during which we can warrant good shadowability properties to chaotic trajectories lying in the chaotic attractor, can be estimated as $\langle\tau\rangle \sim \delta^{-h}$, [45] where δ is the number of precision digits used in numerical computations of chaotic trajectories, and

$$h \equiv \frac{2|\langle\lambda_2(n)\rangle|}{\sigma_1^2} \tag{12}$$

is the so-called hyperbolicity exponent [46], given in terms of the average and variance, respectively, of the distribution $P(\lambda_2(1))$ of the time-1 Lyapunov exponent closest to zero. The latter is related to the variance of the time-n exponent by $\sigma_n^2 = n\sigma_1^2$.

This analytical result was obtained under the assumption that the behavior of the time-n exponents undergoes a biased random walk with a reflecting barrier, the latter being represented by the one-step noise level. The average exponent stands for a bias term in this random walk. Evidently this assumption is roughly valid only if the deterministic correlations in the chaotic orbit are neglected, what restricts the validity of Eq. (12), such that this result must be taken as a numerical estimate rather than a precise value. As a result of (12), it turns out that, as the average time-n exponent goes to zero, the shadowing time practically vanishes. As we go far apart this $\tilde{c}_2$ critical value, however, the shadowing time increases again, such that the validity of computer-generated chaotic trajectories is regained, from the shadowability point of view.

6. Conclusions

The cardiac rhythm is basically generated by two pacemakers, a normal and an ectopic one, which should work in synchrony in order to yield a heartbeat stable over large periods of time. How do these pacemakers synchronize their rhythms is a rather difficult question to answer in a direct way, since a biochemical modeling of the membrane–ion interactions would lead to high-dimensional dynamical systems for which the investigation of synchronized behavior is hampered by the large dimensionality of the phase space. A simpler way to proceed would be to choose a phenomenological model for the heartbeat which retains some essential features of the problem, namely the existence of self-sustained relaxation oscillations, with flexibility to allow for many kinds of behaviors, both periodic and chaotic, by varying system parameters. Accordingly, each pacemaker was modeled by a Van der Pol equation, which fulfills these requirements in a very satisfactory way, and which has been used with this purpose for the last 70 years. The advantage in this procedure is to reduce the system dimensionality to a number which can be handled with relative ease with numerical techniques.

The coupling between these oscillators has been modeled in a simple way, more for the sake of simplicity of the resulting equations, rather than a specific physiological reason. The only requirement was the strong or exclusive unidirectional character of the interaction, which turns the coupled system a representative example of the drive-response, or master–slave configuration. Moreover, the pacemakers are non-identical systems, which complicates the analysis of synchronized behavior.

Our results indicate that, for a coupling strength strong enough, one can obtain frequency synchronization for the system. When the oscillators are behaving periodically, which is the most common situation, this reduces to mode-locking. However, as in some intervals of the coupling strength the oscillators are weakly chaotic, the synchronization of chaos implies the near equality of time rates of suitably chosen phases. In the latter case, while one of the pacemakers is periodic and with well-defined frequency, the other pacemaker may undergo chaotic oscillations modulated by the driver oscillator frequency. This has been characterized more properly as rhythm synchronization, or a chaotic modulation of frequencies. If the coupling strength is further increased, there appears a generalized lag synchronization, for which the oscillator amplitudes are mutually different but still lagged by a nearly constant time interval.

The forced case, which would represent the interaction with a third and artificial pacemaker, would not change significantly the above picture, but our results show that the pacemaker dynamics becomes more difficult to synchronize than in the unforced case. Moreover, the addition of a time-periodic term includes a new feature which is the possibility of hyperchaos, which acts mainly against synchronization in general. We have also investigated the shadowing properties of the chaotic and hyper-chaotic trajectories using finite-time Lyapunov exponents. We found that there are intervals for the coupling strength for which there is shadowing breakdown due to unstable dimension variable.

Finally, the assumption of a bidirectional coupling, with strong asymmetry, would not lead to qualitative new results, with respect to the former cases. Even though our conclusions were drawn upon simple low-dimensional oscillator models, we claim that these features would still be present in more complex models for the pacemaker activity, like those based on biochemical modeling of heart cells.

Acknowledgements

This work was made possible through partial financial support from the following Brazilian research agencies: CNPq, and CAPES.

References

[1] D. Van der Pol, J. Van der Mark, Philos. Mag. 6 (1928) 763.
[2] C.R. Katholi, F. Urthaler, J. Macy Jr., T.N. James, Comp. Biom. Res. 10 (1977) 529.
[3] J. Honerkamp, J. Math. Biol. 18 (1983) 69.
[4] L. Glass, Theory of Heart, Springer, New York-Heidelberg-Berlin, 1990.
[5] L. Glass, M.R. Guevara, A. Shrier, R. Perez, Physica D 7 (1983) 89.
[6] M. Courtemanche, L. Glass, J. Bélair, D. Scagliotti, D. Gordon, Physica D 40 (1989) 299.
[7] T.R. Chay, Int. J. Bifurcat. Chaos 5 (1995) 1439.
[8] D. Noble, Chaos, Solit. Fract. 5 (1995) 321.
[9] L. Glass, Nature 410 (2001) 279.
[10] J. Engelbrecht, O. Kongas, Appl. Anal. 57 (1995) 119.
[11] A. Pikovsky, M. Rosenblum, J. Kurths, Synchronization: A Universal Concept in Non-linear Sciences, Cambridge University Press, Cambridge, 2001.

[12] F.B. Saksena, N. Goldshlager, Electrical Therapy of Cardiac Arrhythmias, W. B. Saunders, New York, 1990.
[13] T. Shinbrot, C. Grebogi, E. Ott, J.A. Yorke, Nature 363 (1993) 411.
[14] A. Garfinkel, M.L. Spano, W.L. Ditto, J.N. Weiss, Science 257 (1992) 1230.
[15] G.K. Moe, J. Alife, W.J. Mueller, B.C. Moe, Circulation 56 (1977) 968.
[16] R. De Paola, H.X. Wang, W.I. Norwood, Am. J. Physiol. 265 (1993) H1603.
[17] V. Schulte-Frohlinde, Y. Ashkenazy, P.C. Ivanov, L. Glass, A.L. Goldberger, H.E. Stanley, Phys. Rev. Lett. 87 (2001) 068104.
[18] P.C. Ivanov, M.G. Rosenblum, C.K. Peng, J. Mietus, S. Havlin, H.E. Stanley, A.L. Goldberger, Nature 383 (1996) 323.
[19] P.C. Ivanov, L.A.N. Amaral, A.L. Goldberger, S. Havlin, M.G. Rosenblum, Z.R. Struzik, H.E. Stanley, Nature 399 (1999) 461.
[20] L.S. Liebovitch, A.T. Todorov, M. Zochowski, D. Scheurle, L. Colgin, M.A. Wood, K.A. Ellenbogen, J.M. Herre, R.C. Bernstein, Phys. Rev. E 59 (1999) 3312.
[21] K. Kotani, K. Takamasu, Y. Ashkenazy, H.E. Stanley, Y. Yamamoto, Phys. Rev. E 65 (2002) 051923.
[22] P.C. Ivanov, L.A.N. Amaral, A.L. Goldberger, H.E. Stanley, Europhys. Lett. 43 (1998) 363.
[23] S. Bocalletti, J. Kurths, G. Osipov, D. Valladares, C.S. Zhou, Phys. Rep. 366 (2002) 1.
[24] M.G. Rosenblum, A.S. Pikovsky, J. Kurths, Phys. Rev. Lett. 76 (1996) 1804;
A.S. Pikovsky, M.G. Rosenblum, G.V. Osipov, J. Kurths, Physica D 104 (1997) 219.
[25] D.V. Anosov, Proc. Steklov Inst. Math. 90 (1967) 1.
[26] R. Bowen, J. Differential Equations 18 (1975) 333.
[27] C. Grebogi, S. Hammel, J.A. Yorke, J. Complexity 3 (1987) 136;
C. Grebogi, S. Hammel, J.A. Yorke, Bull. Am. Math. Soc. 19 (1988) 465;
C. Grebogi, S. Hammel, J.A. Yorke, T. Sauer, Phys. Rev. Lett. 65 (1990) 1527.
[28] R. Abraham, S. Smale, Proc. Symp. Pure Math. (AMS) 14 (1970) 5.
[29] Y.-C. Lai, C. Grebogi, Int. J. Bifurcat. Chaos 10 (2000) 683.
[30] S.P. Dawson, C. Grebogi, T. Sauer, J.A. Yorke, Phys. Rev. Lett. 73 (1994) 1927.
[31] J. Guckenheimer, P.J. Holmes, Nonlinear Oscillations, Dynamical Systems, and Bifurcations of Vector Fields, Springer, New York, 1983.
[32] M.G. Rosenblum, A.S. Pikowsky, J. Kurths, Phys. Rev. Lett. 78 (1997) 4193.
[33] A. Pikovsky, M. Rosenblum, J. Kurths, Int. J. Bifurcat. Chaos 10 (2000) 2291.
[34] S.E. de S. Pinto, S.R. Lopes, R.L. Viana, Physica A 303 (2002) 339.
[35] J. Kurths, S. Boccaletti, C. Grebogi, Y.-C. Lai, Chaos 13 (2003) 126.
[36] Z. Zheng, Gang Hu, Phys. Rev. E 62 (2000) 7882.
[37] L. Glass, W. Zeng, Int. J. Bifurcat. Chaos 4 (1994) 1061.
[38] A.S. Pikovsky, Z. Phys. B 55 (1984) 149.
[39] C. Grebogi, L. Poon, T. Sauer, J.A. Yorke, D. Auerbach, in: B. Fiedler (Ed.), Handbook of Dynamical Systems, Vol. 2, Elsevier, Amsterdam, 2002, (Chapter 7).
[40] Y.-C. Lai, C. Grebogi, J. Kurths, Phys. Rev. E 59 (1999) 2907.
[41] H.D.I. Abarbanel, R. Brown, M.B. Kennel, J. Nonlinear Sci. 1 (1991) 175.
[42] E.J. Kostelich, I. Kan, C. Grebogi, E. Ott, J.A. Yorke, Physica D 109 (1997) 81.
[43] R.L. Viana, C. Grebogi, Phys. Rev. E 62 (2000) 462.
[44] R.L. Viana, C. Grebogi, Int. J. Bifurcat. Chaos 11 (2001) 2689.
[45] T. Sauer, C. Grebogi, J.A. Yorke, Phys. Rev. Lett. 79 (1997) 59.
[46] T. Sauer, Phys. Rev. E 65 (2002) 036220.